

Discriminating cosmic muons and radioactivity using a liquid scintillation fiber detector

Y.P. Zhang,^{a,b,1} J.L. Xu,^a H.Q. Lu,^a P. Zhang,^a C.C. Zhang,^a and C.G. Yang^a

^a*Institute of High Energy Physics, Chinese Academy of Sciences, Yuquan Road, Beijing, 100049, China*

^b*University of Chinese Academy of Sciences, Yuquan Road, Beijing, 100049, China*

E-mail: ypzhang1991@ihep.ac.cn

ABSTRACT: In the case of underground experiments for neutrino physics or rare event searches, the background caused by cosmic muons contributes significantly and therefore has to be identified and rejected. We were proposing and optimizing a new detector using liquid scintillator with wavelength shifting fibers to read out which can be employed as a veto detector for cosmic muon background rejection. The prototype detector was located in laboratory of the institute of high energy physics (IHEP). From the prototype study, it has been found that the detector has good performances and is capable to discriminate between muon induced signal and environmental radiation background. The muon detection efficiency is greater than 98% and, on average, 58 photo-electrons are collected when a muon is going through the detector. To optimize the design and enhance the collected light, the reflectivity of coating materials has been studied in detail. A Monte Carlo simulation of the detector has been developed and compared to the performed measurements showing a good agreement between data and simulation.

KEYWORDS: Liquid detectors, Scintillators, Detector design

¹Corresponding author.

Contents

1	Introduction	1
2	Experimental setup	3
2.1	Prototype detector construction	3
2.2	PMT calibration	4
2.3	Detector response and efficiency for muon	4
3	Light yield of LSF detector	6
3.1	Influence of liner reflectivity	6
3.2	Influence of LS thickness	8
4	Background discrimination capability	9
5	Conclusion and discussion	9

1 Introduction

The basic working principle of a Liquid Scintillator with Fiber (LSF) detector is shown in Fig.1. An optical sealed container is filled with Liquid Scintillator (LS) and a WaveLength Shifting (WLS) fiber, placed in the centre of the container, is connected at both ends to standard PhotoMultiplier Tubes (PMT). Ionizing radiation going through the LS will generate optical photons, which will be eventually collected by the fiber and read out at both ends by PMTs. Multiple containers are put together to composed a layer. A packing of multiple layers makes a particle detector with tracking capabilities.

LSF detectors have been successfully employed in neutrino physics experiments thanks to their very good performances and moderate costs. It was one of the detector option for the MINOS [1] experiment at Fermilab and it has been selected, as an example, for the NOvA [2, 3] longbaseline neutrino experiment. The NOvA detector is made of 344,000 cells of extruded, highly reflective plastic PVC filled with LS and readout by a WLS fiber connected to Avalanche Photo-Diodes. Using the pattern of light seen by the photo-detectors, what kind of neutrino caused the interaction and what its energy was can be determined. One of the main reasons to use such detector technology for neutrino physics is due to the capability of covering large areas with moderate costs obtaining very good tracking performances. This is expecially relevant for underground neutrino or dark-matter searches experiments where large areas have to be covered.

For the underground large-scale particle physics experiment, due to low signal rates and large volume of detector, the background caused by cosmic ray muon is the main background. Although the purpose of NOvA detectors is not measuring cosmic muon

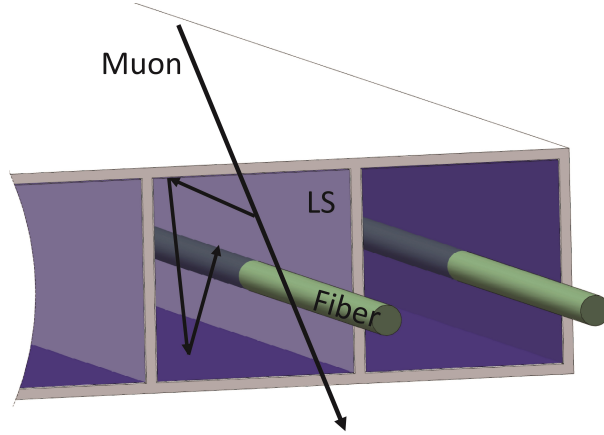


Figure 1. LSF detector working principle.

background, the optimized LSF detector also can be used as veto detector which can reject radioactivity background from surrounding rock and tag cosmic muons in underground neutrino experiment or underground dark matter experiment. According to cosmic muons event rate and radioactivity background level, thickness of LS and number of LSF detector can be adjusted so that the detector has the ability to distinguish between cosmic rays signal and radioactive background signal. Recently, the LSF technology was proposed as an option to be used for the veto detector of the Jiangmen Underground Neutrino Observatory (JUNO) experiment [4]. The JUNO [5] detector, under construction in a 700 m.w.e. underground lab, will exploit the neutrino mass hierarchy by measuring the reactor anti-neutrino spectrum in a large (20 kt) liquid scintillator detector. JUNO is a multi-purpose detector and will address several neutrino physics topics, such as measurement of the neutrino oscillation parameters, and it will exploit the solar, atmospheric and supernova neutrinos physics. Background rejection (environmental radioactivity and cosmic rays induced background) is therefore a crucial issue to fully exploit the physics potential of JUNO. Neutrino detectors are located in deep underground lab and combined with veto detectors for cosmic muon background rejection.

If LSF detectors are compared to other tracking devices, for instance Resistive Plate Chambers (RPC) [6], the former show much smaller dependence on the environmental parameters (i.e. temperature and humidity). Moreover their maintenance and operation is easier compared to gaseous detectors. Moreover the successful production and excellent performance of LS in Daya Bay neutrino experiment [7] prove that the condition is mature for LSF detector fabrication in China.

In the following the structure of a LSF prototype is described and its performances discussed in details. The results show that the technology is perfectly adequate to the physics requirements of a veto detector for underground physics.

2 Experimental setup

2.1 Prototype detector construction

Figure 2 shows the schematic of LSF prototype module. The container box, with a size of about $100 \times 25 \times 12 \text{ cm}^3$, is filled with LS [8–10]. The BCF-92 type wavelength shifting fibers with diameter 1.5 mm and multi wrapped from Saint-Gobain company [11] are placed inside the container. The fiber is readout by two Hamamatsu PMTs (R7600U-100-M4) with four windows and a high gain of about 5×10^6 [12]. The container base material is PVC thanks to the high compatibility with LS and relatively cheap price. To enhance the light reflectivity of the internal container walls, PVC has been mixed with titanium dioxide as the container and reflector. It is well known that pure PVC and TiO_2 are compatible with LS, but if employed in a mixture with other auxiliary materials, it may reduce or even jeopardize the compatibility with LS. Therefore the ratio of these materials was adjusted to make sure that the PVC strength is maintained and performance is good with more TiO_2 and less auxiliary materials. The overall optical performances as a function of TiO_2 content has been optimized.

Several PVC samples from Rifeng factory [13] in Foshan city, have been studied and LS compatibility and reflectivity tests have been performed. Eventually, PVC type 1071 was chosen as the prototype container material. The reflectivity of PVC type 1071 is shown in Fig. 6.

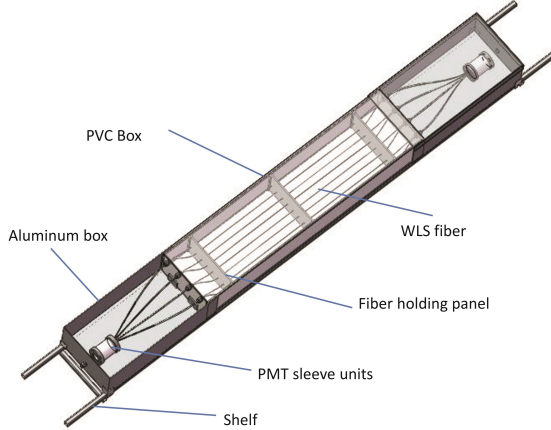


Figure 2. LSF prototype detector schema.

As shown in Fig. 2, the LS container internal part has been split into several narrow units which has been used to test different position reconstruction resolution. Eight WLS fibers were uniformly immersed into LS for light collection. According to MINOS experience [1], the corners and middle positions where the fibers have been placed can cause a 10% variance in the p.e. collection. In order reducing light loss, the cross section of the fibers was lapped. After fibers assembly, both ends of PVC container were covered by an aluminum box. To guarantee a good coupling to the fibers, the PMT was put in a sleeve and afterwards inside an aluminum box. Two LEDs were placed close to both PMTs for

gain calibration. The readout signal cables and the PMT power supply cables exit from the aluminum boxes and the whole prototype module was made light-tight. Finally, the LSF prototype module has been placed between three layers of plastic scintillators which were used as a cosmic ray telescope to trigger signals coming from going through muons. The signals were recorded with an oscilloscope.

The whole process of detector construction and assembly was kept as clean as possible to reduce impurities. All parts were cleaned using deionized water in an ultrasonic bath.

2.2 PMT calibration

With the PMT put into a dark box, a dark current of about 321 uA (max 400 uA), with an applied voltage of 880 V (max 900V), has been measured. The two PMTs coincidence noise rate of about 0.55 Hz has been measured with a 200 ns time window and a 3 mV signal threshold; increasing the threshold to 4 mV, the coincidence rate reduces to less than 0.01 Hz. The PMT calibration was performed using a LED in a dark box and driven by a pulse generator. The PMT waveforms were recorded by oscilloscope with a 100 ps time resolution. For each PMT, different LED intensities have been used to calibrate the PMT single p.e. peak and to get reliable results which is the average of different gains under different LED intensities.

Figure 3 shows the signal PMT charge spectrum after waveform integration. Assuming a certain PMT response model [14], by fitting the single p.e. spectrum, the single p.e. peak with charge Q1 of about 0.93 pC is obtained. The gain calibration was performed twice, before and after each measurement. The gains of two PMTs are $(4.9 \pm 0.1) \times 10^6$ and $(5.6 \pm 0.3) \times 10^6$, respectively.

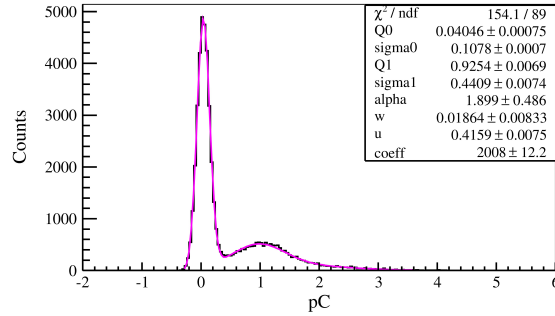


Figure 3. The single p.e. spectrum of the PMT was obtained by the LED calibration in LSF prototype detector. The spectrum was fitted using a PMT response function described in [14].

2.3 Detector response and efficiency for muon

Cosmic ray muons go through the LS, deposit some energy which produces scintillation photons which are collected by the fibers and transmitted to the PMTs. If the number of collected p.e. is high enough, it allows to set an higher discrimination threshold and obtain a better signal-to-noise ratio. Several factors influence p.e. collection, such as LS attenuation length, LS thickness, container reflectivity, WLS fibers attenuation length,

PMT quantum efficiency, WLS fiber to PMT coupling, and others. Due to the compact detector geometry of the prototype, photons can only travel dozens centimeters after several reflection. According to the previous study [10], the LS attenuation length is greater than 10 m, and therefore influence caused by LS attenuation length can be neglected.

The signals coming from three scintillators used as the telescopes were transmitted into a low threshold discriminator module with threshold of 25 mV. The discriminator gave a coincident signal that was used as a trigger input to the oscilloscope. Figure 4 shows the waveform signal recording logical diagram for offline analysis.

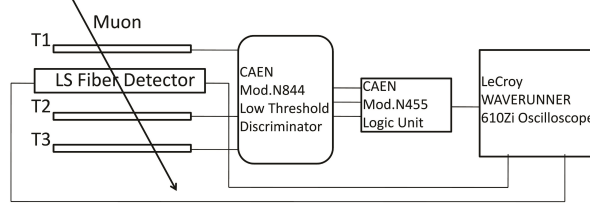


Figure 4. Signal waveform recording logical diagram, T1, T2 and T3 indicate the plastic scintillators of the cosmic ray telescope.

When muons go through several centimeters of a material, the ionization energy loss obeys a Landau distribution while the number of optical photons LS emitted follows the Gaussian function. As can be seen in Figure 5, the energy spectrum collected for the passing muons has been fitted to a Landau convoluted Gaussian distribution. The most probable value for the number of photo electrons, with 8 cm LS depth, is 58 p.e. The value has been obtained while the LSF module used PVC as reflector, without the use of additional reflector materials.

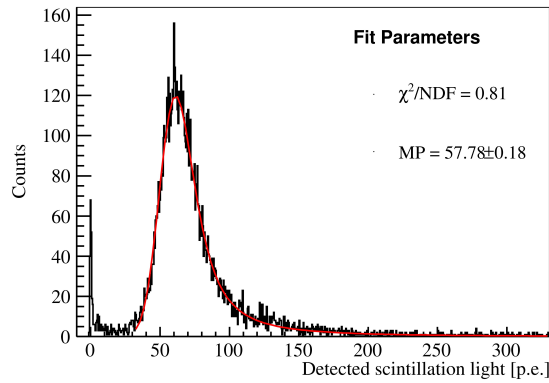


Figure 5. Detector response for passing muons

As shown in Figure 4, one plastic scintillator pad was placed above the prototype module and two were placed underneath. All telescopes were vertically aligned along the

shelf. The sensitive areas of telescope pads are smaller than the LS active area which will keep all selected muons passing through LS. The detection efficiency and its statistics error have been calculated with the following functions:

$$\epsilon = \frac{N_{T1\&T2\&T3\&PMT1\&PMT2}}{N_{T1\&T2\&T3}} \quad (2.1)$$

$$\sigma = \sqrt{\frac{\epsilon(1 - \epsilon)}{N_{T1\&T2\&T3}}} \quad (2.2)$$

Where T1, T2 and T3 are three telescope pads, respectively. PMT1 and PMT2 are the PMTs at the both ends of LSF detector. The numerator in equation 2.1 is the number of counts of the coincidence among the three telescope pads and the two PMTs, over a 100 ns time window. The denominator is the number of counts of coincidence among the three telescopes pads. The signals coming from the telescope pads and the PMTs were transmitted into a low threshold discriminator with 25 mV thresholds for the telescope pads and 4mV for the LSF detector, respectively. An higher threshold for the trigger has been used to reduce coincidence noise from plastic scintillator. The measured detector efficiency is about $98.6 \pm 0.1\%$. The small inefficiency is due to the dead areas in the LSF detector: the fiber holding panel structure in the LS and the WLS fiber bending before going out the LS.

3 Light yield of LSF detector

3.1 Influence of liner reflectivity

In order to increase the collected number of p.e., different materials, compatible with the LS, were added as reflector in the LSF container. ESR and PTFE were selected as coating material for the inner walls of the container. Figure 6 shows the reflectivity of PVC, ESR and PTFE. The PTFE reflectivity decreases with increasing wavelength, while the ESR and PVC reflectivity show a step-like function having very low values below 380nm, and reaching a high value (greater than 95% in case of ESR) with increasing wavelength.

The wavelength peak of Daya Bay LS emission spectrum lays between 400 and 440 nm, but the p.e. collection of ESR with highest reflection in measurement turned out to be much lower than that of PVC and PTFE. Previous studies [16] have shown that ESR reflectivity depended on the photon incidence angle when ESR was immersed in mineral oil. Therefore an experiment to measure the ESR film reflectivity has been performed. The schematic of the ESR reflectivity measurement is shown in Fig. 7: a photon beam produced by an ad hoc wavelength LED was transmitted through an optical fiber, focused and made parallel after exiting the optical fiber. Photons reflected by the ESR are finally detected by the PMT.

During the process, a reference measurement has been taken before immersing the ESR sample in the LS. After having inserted vertically the ESR sample in a quartz glass cup, filled with mineral oil, the reflectivity measurement was taken. The PMT could be rotated of an arbitrary angle to match and measure the reflected light. The collected charge has

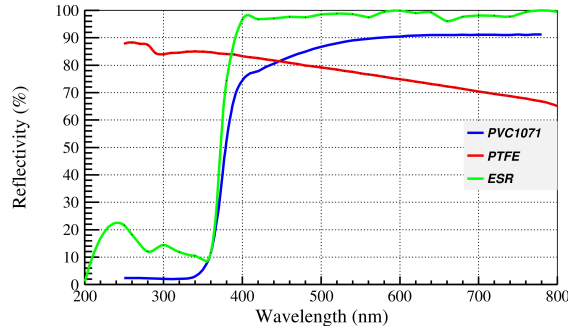


Figure 6. Different material reflectivity. A Special PVC, type 1071 produced by Rifeng Co. Ltd [13]. The PVC and PTFE reflectivity are measured in air by International Institute of Metrology, China [15]. ESR reflectivity data come directly from the producer data sheet.

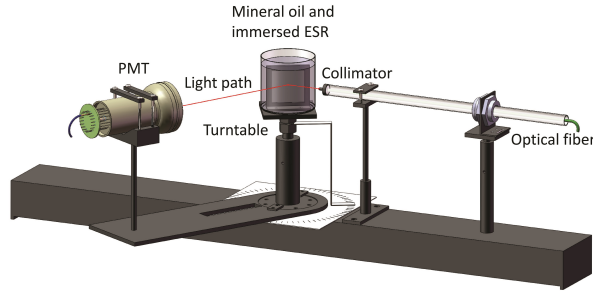


Figure 7. ESR reflectivity measurement schematics.

been finally integrated by a QDC (Charge-to-Digital Converter). The measured reflectivity, R , can be expressed by the following equation:

$$R = \frac{Q_2 - Q_0}{Q_1 - Q_0} \quad (3.1)$$

where Q_0 is the measured charge with the LED off, therefore it is the background normalization of the measurement. Q_1 is the charge without ESR which expresses incident light intensity, and Q_2 is the reflected light charge. Figure 8 shows the measured ESR reflectivity as a function of the incident photon angle.

A ESR reflectivity value of about 90% is reached when the incident angle becomes smaller than 65 degrees and exhibit a sharp decrease to about 50% for larger incident angles. The reflectivity measurement was repeated systematically for other wavelength LEDs, ranging from 365nm to 600nm, with a 20nm step interval. A similar behaviour was observed, as a function of the incident angle, for each LED. As a final comment on reflectivity, when incident angle becomes smaller than 65 degree, Figure 8 shows the obtained value is lower than that given in the ESR data sheet. The discrepancy is likely caused by light

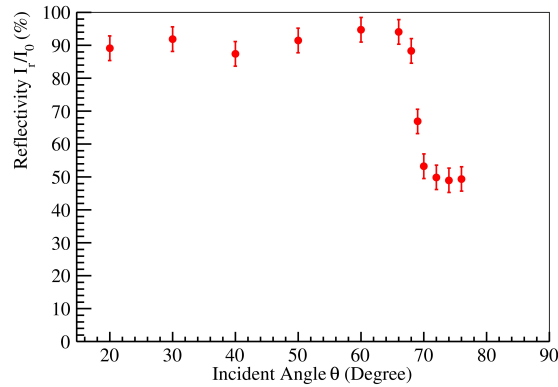


Figure 8. ESR reflectivity with different incident angle. The optical source is an LED with center value 416nm (sigma 8nm). For every point in the diagram, the error on the angle is about 0.5 degree.

transmission losses and diffusion reflections, non corrected for, when light goes through different media.

In order to better understand detector performances, a Monte Carlo (MC) simulation in the Geant4 [17] framework has been implemented. The measured reflectivity data were input into simulation. Simulation of PTFE, PVC and ESR coating of the internal container walls has been implemented and brings simulation results which are consistent with the measurements. Simulation and experiment measurement results are shown in table 1.

Table 1. P.e. collection results with different materials obtained by measurement and simulation.

Material	Exp. (p.e.)	Sim. (p.e.)
PVC	57.8	57.7
PTFE	72.5	68.3
ESR	46.7	50.5

3.2 Influence of LS thickness

Silicone oil was painted on the fiber cross section to improve the coupling between the WLS fiber and the PMT photocathode window. The operation increased the number of collected p.e. by almost 10%. As we know, the thicker the LS, the higher the number of collected p.e. in the detector, making it easier to discriminate between muons and environmental radioactivity. The relationship between the LS thickness and the number of collected p.e. was studied since it can be relevant to optimize future detector designs.

We set several depths of LS with PTFE material as reflector to study detector response. Figure 9 shows the number of collected p.e. as a function of the LS thickness in the LSF detector. The results are compared to the Monte Carlo simulation and show that the results are consistent.

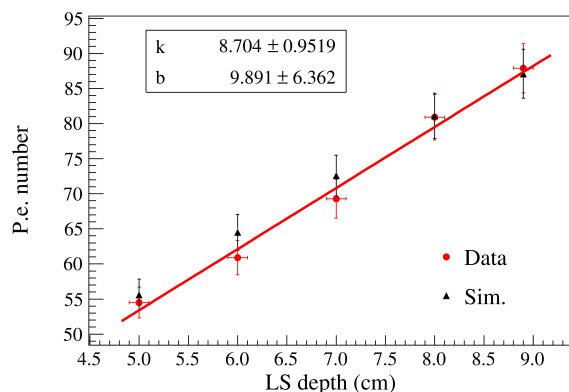


Figure 9. Number of collected p.e versus the LS thickness. Data are compared to the Monte Carlo simulation.

The number of collected p.e. exhibit an almost linear behaviour as a function of the LS thickness. Data have been fitted with a linear function and show an increment of about 8.7 p.e. every increase of 1cm in the LS thickness.

4 Background discrimination capability

If the LSF detector is chosen as an option for a veto detector, cosmic ray muons deposit roughly ~ 2 MeV per centimeter in the LS, while environmental radioactivity is below 3 MeV. Relatively thick liquid scintillator can effectively distinguish muons from radioactivity background which comes from the surrounding rock. Muon and rock radioactivity response in simple LS detector were simulated, as can be shown in Fig. 10. With a 8cm thick LS, the average number of collected p.e. is about 60, while all the radioactivity events from the surrounding rock induce a much lower number of p.e. in the detector. By cutting the events using a 25 p.e. threshold, the muon selection efficiency is larger than 98%. Since the single rate of environmental radioactivity surviving the cut is about 200 Hz, multi-layers of detector can be used to suppress further the environmental radioactivity. The noise to signal ratio will be smaller than 0.1% assuming two layers coincidence. The result satisfies the JUNO veto detector requirement [4], therefore the LSF detector developed and studied in the the present paper could be chosen as top veto tracker for the JUNO experiment.

5 Conclusion and discussion

A Liquid Scintillator with WaveLength Shifting fiber prototype detector has been designed, built, and its performances studied in details. It has been shown that such detector could serve well in identifying cosmic muons traversing the detector and distinguish them from environmental radiation, such as gamma. An average number of 58 p.e. are collected for passing muons, with a detection efficiency greater than 98%. To enhance the reflectivity of the inner walls of the detector, several coating materials have been studied.

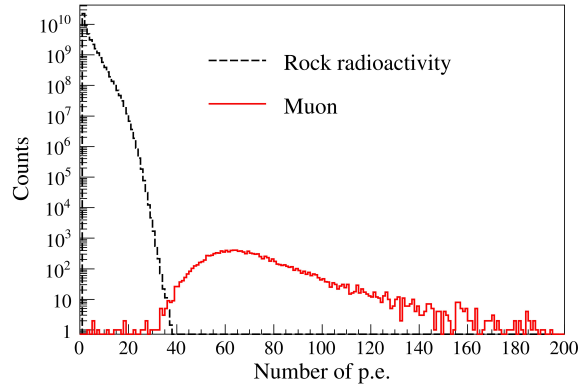


Figure 10. Rock radioactivity and muon response in a detector with 8 cm LS thickness in simulation.

By the prototype study, the p.e. collection of ESR with highest reflection is much lower than PVC and PTFE collection. For the results, the ESR reflectivity has been further investigated and dedicated measurements have been performed immersing a ESR film in mineral oil and measuring the reflectivity as a function of the incident angle. The measurement shows that the ESR reflectivity is a sharp function of the incident angle being lower with large incident angle than reflectivity with small incident angle.

Detector with PTFE reflectors shows better performances and 25% more p.e. collection than with PVC reflectors. PTFE is better suited for the purposes with respect to PVC and ESR. PTFE used as detector container is a good candidate for the future detector designs.

By optimizing the geometry layout structure of the detector, the p.e. collection can be made higher than that of the NO ν A detector [18] with a superior noise to signal ratio due to the thicker LS in the detector.

Thanks to the outstanding performances of the LSF detector, it has been proposed as an option for the top veto detector of the JUNO experiment. LSF detector definitely can satisfy JUNO requirement.

The study can serve as a reference and guideline for future underground low background experiments or accelerator experiments planning to use similar LSF detectors.

Acknowledgments

This work was supported by the Strategic Priority Research Program of the Chinese Academy of Sciences(Grant No.XDA10010300).

References

- [1] P. Border et al., 2001 A large liquid scintillator detector for a long baseline neutrino oscillation experiment, Nucl. Inst. Meth. A **463** 194
- [2] D.S. Ayres et al., Technical Design Report, FERMILAB-DESIGN-2007-01

- [3] S. Phan-Budd, 2012 Construction of PVC extrusions for the NO ν A near and far detectors, Physics Procedia **37** 1201
- [4] JUNO Collaboration, T. Adam et al., JUNO Conceptual Design Report, arxiv:1508.07166
- [5] JUNO Collaboration, F.P. An et al., 2016 Neutrino physics with JUNO, J. Phys. G **43** 030401
- [6] J.L. Xu et al., 2011 Design and preliminary test results of Daya Bay RPC modules, Chin. Phys. C **35** 844
- [7] Daya Bay Collaboration, F.P. An et al., 2012 Observation of electron-antineutrino disappearance at Daya Bay, Phys. Rev. Lett. **108** 171803
- [8] Y.Y. Ding et al., 2007 Research and development of gadolinium loaded liquid scintillator for Daya Bay neutrino experiment, Journal of Rare Earths **25** 310
- [9] M. Yeh et al., 2007 Gadolinium-loaded liquid scintillator for high-precision measurements of antineutrino oscillations and the mixing angle, θ_{13} , Nucl. Inst. Meth. A **578** 329
- [10] Y.Y. Ding et al., 2008 A new gadolinium-loaded liquid scintillator for reactor neutrino detection, Nucl. Inst. Meth. A **584** 238
- [11] Organic Scintillation Materials and Assemblies, <http://www.crystals.saint-gobain.com/sites/imdf.crystals.com/files/documents/organics-brochure.pdf>, 03/01/2017
- [12] Photomultiplier Tube R7600U-100-M4 Datasheet, <http://www.hamamatsu.com/us/en/R7600U-100-M4.html>
- [13] <http://www.rifeng.com.cn/>, last access: 03/01/2017
- [14] E.H. Bellamy et al., 1994 Absolute calibration and monitoring of a spectrometric channel using a photomultiplier, Nucl. Inst. Meth. A **339** 468
- [15] <http://www.nim.ac.cn/>, last access: 03/01/2017
- [16] N. Jimmy et al., Reflectivity of 3M ESR and miro-silver at different incident angle, <http://dayabay.ihep.ac.cn/cgi-bin/DocDB/ShowDocument?docid=1619>, last access: 03/01/2017
- [17] <http://geant4.cern.ch/>, last access: 03/01/2017
- [18] NO ν A Collaboration, D.S. Ayres et al., NuMI off-axis ν_e appearance experiment, http://www-nova.fnal.gov/NOvA_Proposal/NOvA_P929_March21_2005.pdf, last access: 03/01/2017